Title

Wavelet Deep Learning Network for Objective Retinal Functional Estimation from Multimodal Retinal Imaging

ISBN

9783031731181

Authors

Le, An D

Yassin, Shaden H

Freeman, William R

et al.

Publication Date

2025

DOI

10.1007/978-3-031-73119-8_4

Wavelet Deep Learning Network for Objective Retinal Functional Estimation from Multimodal Retinal Imaging

An D. Le[1], Shaden H. Yassin[2], William R. Freeman[2], Anna Heinke[2], Dirk-Uwe G. Bartsch[2], Shyamanga Borooah[2], Shiwei Jin[1], Truong Nguyen[1], and Cheolhong An[1]

[1] Electrical and Computer Engineering Department, University of California San Diego, La Jolla, CA 92093, USA
{d0le,sjin,tqn001,chan}@ucsd.edu

[2] Jacobs Retina Center, Shiley Eye Institute, University of California San Diego, La Jolla, CA 92093, USA
{syassin,wrfreeman,aheinke,dbartsch,sborooah}@health.ucsd.edu

Abstract. In this study, we proposed a wavelet-based deep learning network to estimate retinal function from retinal structure in patients with Retinitis Pigmentosa. We used macular integrity assessment microperimetry to measure retinal sensitivities (functional information) and spectral domain optical coherence tomography to assess retinal layer thicknesses (structural information). Outer, inner, and total retinal thicknesses were extracted. We found a strong correlation between outer retinal thickness and retinal sensitivity. Leveraging this correlation, we employed machine learning models for functional estimation from retinal layer thicknesses and vice versa. For functional estimation, we incorporated discrete wavelet transform and max-pooling features in a ResNet18-based architecture, significantly improving the accuracy to an R^2 score of 0.79. Our results demonstrate that machine learning models can effectively predict retinal function from retinal structure, and vice versa. Furthermore, the integration of discrete wavelet transform features in the convolutional neural network improved the performance of functional estimation from retinal structure.

Keywords: Biomedical image processing · Retinal images · Multi-modal · Machine learning · Convolutional neural networks · Residual neural networks · Discrete wavelet transforms.

1 Introduction

Our main goal is to investigate and develop machine learning models capable of estimating retinal function from retinal structure and vice versa. Many clinical studies show the strong link between changes in retinal structure and function, crucial for monitoring various pathologies. Spectral domain optical coherence tomography (SD-OCT) has proven invaluable in detecting abnormal macular thick-

ness in children [15] and monitoring disease progression in conditions like Retinitis Pigmentosa (RP) and Usher syndrome [12, 13]. Macular integrity assessment (MAIA) microperimetry subjectively measures retinal sensitivity changes in clinical trials [3, 8]. There is increasing interest in studying the relationship between retinal structure from SD-OCT and function from microperimetry. Further studies have identified a strong structure-function relationship in glaucoma using SD-OCT and microperimetry, showing significant correlations in RP patients between retinal structure and function changes [1, 6, 9]. Additionally, research is focusing on developing predictive tools for retinal function based on structural data, such as the work in [11] for patients with glaucoma.

Our study proposes an innovative machine learning technique named the Hybrid Wavelet Pooling Unit (HyWaPU). The proposed method integrates the Discrete Wavelet Transform (DWT) [4, 14] into CNNs, leveraging DWT's advantages in solving other computer vision problems [10]. HyWaPU significantly improved the ability of convolutional neural networks (CNN) to objectively predict sensitivity from retinal thickness data. The correlation we found between retinal structure and function in RP patients supports the use of retinal structure in estimating retinal function. The study also demonstrates the reliability of machine learning models to predict retinal function from structural measurements like total (TRT), outer (ORT), and inner (IRT) retinal, and vice versa. We also discovered a strong correlation between ORT and changes in sensitivity, likely due to the loss of photoreceptor cells in patients with RP.

2 Literature Review

Recent clinical studies have investigated the relationship between retinal structure and function in patients with glaucoma and RP using multimodal imaging from various optical instruments. The clinical work in [15] found that there is an association between cone density and visual funcion in patients with RP. In [9], both circumpapillary microperimetry sensitivity and circumpapillary retinal nerve fiber layer thickness measured by SD-OCT showed comparable diagnostic efficacy in identifying glaucoma patients, indicating a robust structure-function relationship. Nevertheless, a limited number of studies, such as [6] and [1], quantitatively demonstrate strong correlations between retinal structural changes, particularly in ORT, and retinal sensitivity changes in RP patients. In addition, the work in [11] developed an artificial intelligence based approach to predict retinal function from retinal structure for patient with glaucoma. In this study, we proposed a novel approach for CNNs to estimate function from retinal structure in patients with RP. We also employed various AI techniques to predict structure from the functional information. As far as we know, this is the first work showing the reliability of AI mapping retinal structure and function for patients with RP. We also found a strong structure-function correlation, which supports our AI results.

3 Method

In this study, we initially examined the relationship between retinal structure and function using correlation coefficients. We aligned MAIA-NIR images with OCT-IR images and extracted TRT, ORT, and IRT for each MAIA sensitivity spot. Then, we used AI methods to predict sensitivities from retinal thickness and vice versa, focusing on single MAIA sensitivity spots. Our experiments included linear and polynomial regressions, and random forest models. We also utilized window-based approaches with different window sizes and with random forest and ResNet18 models. Finally, we proposed HyWaPU on ResNet18 for further enhancement, achieving the best outcomes.

3.1 Retinal Structure-Function Correlation

The correlation process starts with aligning MAIA-NIR and OCT-IR images, followed by extracting TRT, ORT, and IRT values from SD-OCT data. These, along with retinal sensitivities from MAIA microperimetry, are used to calculate correlation coefficients between sensitivities and retinal thickness parameters.

Alignment Step In our study, we aligned OCT-IR images (768x768 pixels) with MAIA-NIR images (1024x1024 pixels) due to their differing dimensions. This alignment involved using a transformation matrix to align MAIA sensitivity spots with the OCT-IR images, aiding in the accurate extraction of TRT, ORT, and IRT values at these spots. We employed the coarse alignment method outlined in [16, 17], which segments retinal vessels from both image types and uses the SuperPoint network [5] to identify keypoints within these vessels. These keypoints help compute a perspective transformation matrix that effectively aligns the two images.

Correlation Step After aligning the images, we analyzed the correlation between retinal thickness parameters (TRT, ORT, and IRT) and retinal sensitivities. The retinal structure-function relationship was evaluated using correlation coefficients, calculated as follows:

$$r = \frac{\sum (x_i - \bar{x})(y_i - \bar{y})}{\sqrt{\sum (x_i - \bar{x})^2 (y_i - \bar{y})^2}}, \tag{1}$$

in which r represents the correlation coefficient, where x_i and y_i denote values of the first and second variables in a sample, respectively. Furthermore, $\bar{x}$ and $\bar{y}$ represent the means of the values of the first and second variables.

3.2 AI Predictive Tool Study

Single-Point Approach Initially, estimation was conducted using information from a single MAIA sensitivity spot with corresponding coordinates. For

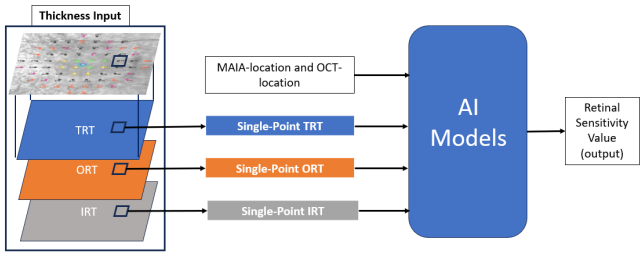

Fig. 1. Visualization of the sensitivity estimation pipeline with TRT, ORT, IRT, and the corresponding MAIA-location and OCT-location as inputs.

the single-point approach, AI models utilized TRT, ORT, IRT, and the location of the sensitivity point center on MAIA-NIR and OCT-IR as inputs to estimate the corresponding sensitivity value. The estimation pipeline is depicted in Fig. 1. In the sensitivity estimation pipeline, various regression methods were employed, including linear regression, polynomial regression, and random forest models [2]. In the retinal structure estimation pipeline, a similar approach was followed. However, in this case, sensitivity values, along with their MAIA and OCT locations, were used as inputs to predict corresponding TRT, ORT, and IRT values.

Window Approach In the window-based approach, AI models utilized TRT, ORT, and IRT values obtained from a predefined window applied to the OCT data as inputs to estimate corresponding sensitivity values. Given that the original OCT data had only 49 B-scans and 512 A-scans for each sample, we performed linear interpolation to enhance resolution, resulting in 512 B-scans and 512 A-scans. We employed windows of varying sizes to extract TRT, ORT, and IRT values from the OCT data. These extracted retinal thickness measurements served as inputs for the random forest [2], ResNet18 [7], and HyWaPU-ResNet18 models.

HyWaPU The Hybrid Wavelet Pooling Unit (HyWaPU) combines max pooling features with high-pass details from the Discrete Wavelet Transform (DWT). With the wavelet coefficients from a chosen wavelet function, we compute the high-pass and low-pass filter matrices, denoted as $\mathbf{H}$ and $\mathbf{L}$. These matrices are used to find the approximation $\mathbf{X}_{ll}$ as well as the detail components $\mathbf{X}_{lh}$, $\mathbf{X}_{hl}$, and $\mathbf{X}_{hh}$. The computation of $\mathbf{L}$ can be mathematically described as follows:

$$\mathbf{L} = \mathbf{D}\widehat{\mathbf{H}}, \tag{2}$$

where $\mathbf{D}$ is the downsampling matrix and $\widehat{\mathbf{H}}$ is a Toeplitz matrix with filter coefficients of $\mathbf{H}_0(z)$. $\mathbf{H}$ has a similar form as $\mathbf{L}$ with filter coefficients of $\mathbf{H}_0(z^{-1})$.

Using $\mathbf{H}$ and $\mathbf{L}$, $\mathbf{X}_{ll}$, $\mathbf{X}_{lh}$, $\mathbf{X}_{hl}$, and $\mathbf{X}_{hh}$ are computed as follows:

$$\begin{aligned} \mathbf{X}_{ll} &= \mathbf{L}\mathbf{X}\mathbf{L}^T, \quad \mathbf{X}_{lh} = \mathbf{H}\mathbf{X}\mathbf{L}^T, \\ \mathbf{X}_{hl} &= \mathbf{L}\mathbf{X}\mathbf{H}^T, \quad \mathbf{X}_{hh} = \mathbf{H}\mathbf{X}\mathbf{H}^T. \end{aligned} \tag{3}$$

As max pooling effectively retains dominant features but often omits critical high-pass details, HyWaPU incorporates the decomposed detail components $\mathbf{X}_{lh}$, $\mathbf{X}_{hl}$, and $\mathbf{X}_{hh}$ from DWT into the max pooling feature map. This integration uses a one-layer Fully Convolutional Network (FCN) with tunable parameters, allowing the unit to optimally blend both types of features. The final feature map includes max-pooled, denoted as $\mathbf{X}_{max}$, and detailed features from DWT, with combination weights fine-tuned through back-propagation during training. The unit is mathematically expressed as follows:

$$X_p = F'(ReLU(\mathbf{X}_{max}), ReLU(\mathbf{X}_{lh}), ReLU(\mathbf{X}_{hl}), ReLU(\mathbf{X}_{hh})), \tag{4}$$

where F' is the one-layer FCN with tunable weights. As shown in Eq. (4), the decomposed detail components via DWT along with the prominent feature map are first independently processed with *ReLU* functions.

We integrated the proposed units into the ResNet family. For the downsampling and pooling layers, we employed the decomposed components along with the max pooling results as inputs for a one-layer Fully Convolutional Network (FCN). In addition, we substitute the two-stride convolution with a non-stride convolution block followed by the proposed units. The implementation is shown in Fig. 2.

4 Experiments and Results

This study analyzed data from 54 eye samples of 30 RP patients, including 68 MAIA sensitivity points and corresponding SD-OCT measurements, collected at UCSD's IRD clinic between July 2021 and April 2023. The data, which adhered to the Declaration of Helsinki principles, included demographics, BCVA, clinical phenotype, and imaging from Spectralis HRA+OCT and MAIA microperimetry. Criteria required a confirmed RP diagnosis and high-quality, same-day SD-OCT

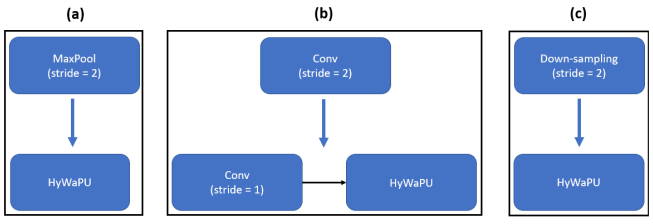

Fig. 2. Implementation of the proposed unit in CNN architectures, replacing max-pool (a), stride-convolution (b), and downsampling (c) functions.

and MAIA assessments, excluding any patients who had eye surgery within the last six months. The data were split into 60% for training and 40% for testing, ensuring distinct separation between the sets. The analysis showed that outer retinal thickness (ORT) strongly correlated with retinal sensitivity, with the HyWaPU-ResNet18 model using a DB3 wavelet achieving an R^2 of 0.79, highlighting its predictive strength.

4.1 Retinal Structure-Function Correlation

In this study, we assessed the relationship between retinal structure and function in RP patients using correlation coefficients. The results revealed correlation coefficients of 0.41 for total retinal thickness (TRT), 0.58 for outer retinal thickness (ORT), and -0.07 for inner retinal thickness (IRT) with corresponding retinal sensitivities. The significant correlation between ORT and retinal function can likely be attributed to the inclusion of photoreceptors in the ORT layer. RP is primarily a photoreceptor degeneration disease. The ORT is mainly composed of photoreceptor cell. Photoreceptors are essential for phototransduction, the process of converting light into electrical signals, marking the initial step in visual perception. Therefore, changes in ORT, such as a reduction or loss, reflect a degeneration of photoreceptors, correlating with a notable reduction in sensitivity as measured by microperimetry. The correlations across all 68 sensitivity spots are visualized in Fig. 3.

4.2 Single-Point Estimation Approach

Sensitivity Value Estimation We employed linear and polynomial regression models using TRT, ORT, IRT, and MAIA/OCT image locations to estimate retinal sensitivities, achieving R^2 values of 0.42 and 0.44, respectively. In the linear model, ORT was highlighted as particularly significant with a weight of 0.91. The most effective model was a random forest with a maximum depth of 10, which attained an R^2 value of 0.519. Detailed results are shown in Table 1.

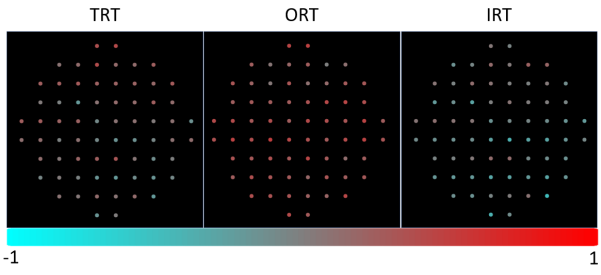

Fig. 3. Visualized distributions of correlation coefficients with the retinal sensitivity values for TRT (left), ORT (middle), and IRT (right). Positive and negative correlations are colorized with hot and cold colors, respectively.

Table 1. Random Forest performance in R^2 with different maximum depth values in estimating retinal thicknesses (TRT, ORT, and IRT) and in estimating retinal sensitivity value.

Models	R^2			
	Thickness Estimation			**Sensitivity Estimation**
	TRT	**ORT**	**IRT**	**Sensitivity**
Random Forest, MaxDepth: 5	0.467	0.547	0.260	0.500
Random Forest, MaxDepth: 10	0.517	**0.602**	**0.329**	**0.519**
Random Forest, MaxDepth: 15	**0.525**	0.594	0.326	0.517
Random Forest, MaxDepth: 20	0.521	0.589	0.322	0.514
Random Forest, MaxDepth: 50	0.520	0.589	0.321	0.513

Retinal Thickness Estimation We utilized random forest regression models with MAIA and SD-OCT locations, along with corresponding retinal sensitivity, to estimate retinal thickness. The best R^2 values for TRT, ORT, and IRT estimations were 0.53, 0.60, and 0.33, respectively. This emphasizes the strong relationship between ORT and retinal sensitivity in RP patients, as ORT estimation showed the highest performance. Performance results for TRT, ORT, and IRT estimations are detailed in Table 1.

4.3 Window Approach for Sensitivity Value Estimation

Random Forest results In this experiment, random forest models predicted sensitivity values at specific window areas using TRT, ORT, and TRT values. Window sizes varied from 11x11 to 191x191. Results, shown in Fig. 4, indicate performance improvement with larger window sizes, plateauing beyond 131x131. The best performance, reaching an R^2 value of 0.599, occurred with a random forest model at a maximum depth of 50 and a window size of 171x171. Moreover, the larger window sizes showed better estimation performances than the single-point estimation approaches, represented with the dots in Fig. 4.

ResNet18 results In this experiment, ResNet18 models utilized TRT, ORT, and TRT values from specific window areas to estimate sensitivity values. Window sizes ranged from 11x11 to 251x251. The performance results of ResNet18 models with different window sizes are shown in Fig. 4. As illustrated, ResNet18 performance improves with larger window sizes. Moreover, in cases with larger windows, ResNet18 models outperform random forest models. The highest performance, with an R^2 value of 0.74, was achieved using the ResNet18 model with a window size of 251x251.

HyWaPU-ResNet18 results In our final experiment, we tested HyWaPU-ResNet18 models integrating various wavelet functions including Haar, DB2, DB3, DB4, Symlet3, and Symlet4, across different window sizes: 11x11, 71x71, 131x131, 191x191, and 251x251. These models were evaluated against the baseline performance of standard ResNet18 models across the same window sizes. The results, illustrated in Fig. 4, show that performance improvements in the

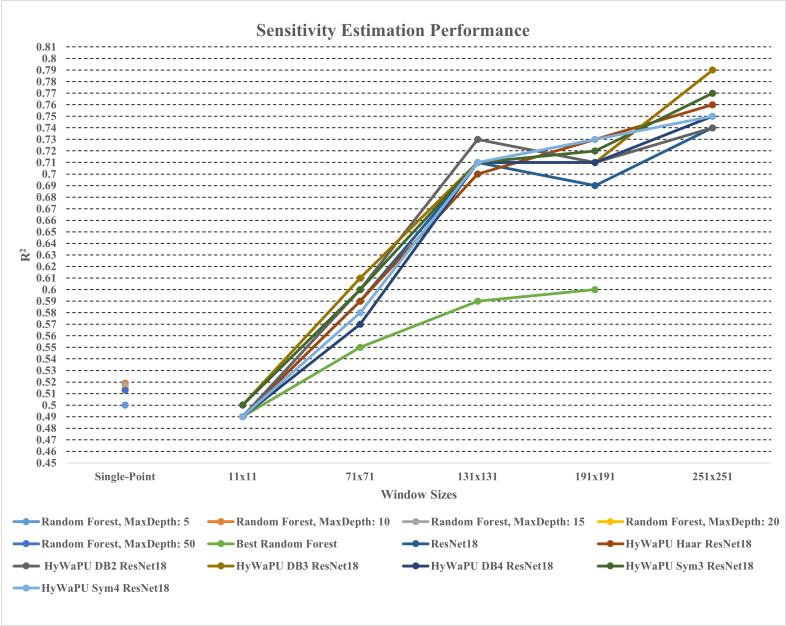

Fig. 4. Visualization of the sensitivity estimation performance in R^2 of random forest, ResNet18 and HyWaPU-ResNet18 models with different window sizes.

HyWaPU-ResNet18 models correlate with increases in window size, with notable gains over the baseline ResNet18, especially at larger window sizes. The best performance was achieved by the HyWaPU-ResNet18 model using the DB3 wavelet in a 251x251 window, reaching an R^2 value of 0.79.

5 Conclusion

In this study, we introduced HyWaPU to improve the performance of the ResNet18 model, significantly enhancing sensitivity estimations. We also examined various machine learning approaches to predict changes in retinal structure and sensitivity, which showed promising results. These findings validate the effectiveness of machine learning models in predicting retinal sensitivity based on structural data and vice versa. In addition, we confirmed a robust relationship between ORT and retinal sensitivity in RP patients using SD-OCT and MAIA microperimetry. Our correlation analysis and structure-function estimations emphasize the importance of the ORT layer, which contains photoreceptors, which are crucial for phototransduction. However, our current methods have not yet successfully estimated retinal structure from functional data, an area we plan to explore in future research. We will also segment photoreceptor parts to confirm if their thinning or loss causes sensitivity drop in RP.

Disclosure of Interests. The authors have no competing interests to declare that are relevant to the content of this article.

References

1. Asahina, Y., Kitano, M., Hashimoto, Y., Yanagisawa, M., Murata, H., Inoue, T., Obata, R., Asaoka, R.: The structure-function relationship measured with optical coherence tomography and a microperimeter with auto-tracking: The mp-3, in patients with retinitis pigmentosa. Scientific Reports **7**(1) (Nov 2017). https://doi.org/10.1038/s41598-017-16143-5
2. Breiman, L.: Machine Learning **45**(1), 5–32 (2001). https://doi.org/10.1023/a:1010933404324
3. Charng, J., Sanfilippo, P.G., Attia, M.S., Dolliver, M., Arunachalam, S., Chew, A.L., Wong, E.N., Mackey, D.A., Chen, F.K.: Interpreting maia microperimetry using age- and retinal loci-specific reference thresholds. Translational Vision Science & Technology **9**(7), 19–19 (06 2020). https://doi.org/10.1167/tvst.9.7.19, https://doi.org/10.1167/tvst.9.7.19
4. Daubechies, I.: Ten Lectures on Wavelets. CBMS-NSF Regional Conference Series in Applied Mathematics, Society for Industrial and Applied Mathematics (1992), https://books.google.com/books?id=B3C5aG4OboIC
5. DeTone, D., Malisiewicz, T., Rabinovich, A.: Superpoint: Self-supervised interest point detection and description. In: 2018 IEEE/CVF Conference on Computer Vision and Pattern Recognition Workshops (CVPRW). pp. 337–33712 (2018). https://doi.org/10.1109/CVPRW.2018.00060
6. Funatsu, J., Murakami, Y., Nakatake, S., Akiyama, M., Fujiwara, K., Shimokawa, S., Tachibana, T., Hisatomi, T., Koyanagi, Y., Momozawa, Y., Sonoda, K.H., Ikeda, Y.: Direct comparison of retinal structure and function in retinitis pigmentosa by co-registering microperimetry and optical coherence tomography. PLOS ONE **14**(12), 1–13 (12 2019). https://doi.org/10.1371/journal.pone.0226097, https://doi.org/10.1371/journal.pone.0226097
7. He, K., Zhang, X., Ren, S., Sun, J.: Deep residual learning for image recognition. In: 2016 IEEE Conference on Computer Vision and Pattern Recognition (CVPR). pp. 770–778 (2016). https://doi.org/10.1109/CVPR.2016.90
8. Jones, P.R., Yasoubi, N., Nardini, M., Rubin, G.S.: Feasibility of Macular Integrity Assessment (MAIA) Microperimetry in Children: Sensitivity, Reliability, and Fixation Stability in Healthy Observers. Investigative Ophthalmology & Visual Science **57**(14), 6349–6359 (11 2016). https://doi.org/10.1167/iovs.16-20037, https://doi.org/10.1167/iovs.16-20037
9. Kita, Y., Hollo, G., Saito, T., Murai, A., Kita, R., Hirakata, A.: Circumpapillary microperimetry to detect glaucoma: A pilot study for sector-based comparison to circumpapillary retinal nerve fiber layer measurement. International Ophthalmology **39**(1), 127–136 (Dec 2017). https://doi.org/10.1007/s10792-017-0796-8
10. Le, A.D., Jin, S., Bae, Y.S., Nguyen, T.: A novel learnable orthogonal wavelet unit neural network with perfection reconstruction constraint relaxation for image classification. In: 2023 IEEE International Conference on Visual Communications and Image Processing (VCIP). pp. 1–5 (2023). https://doi.org/10.1109/VCIP59821.2023.10402772
11. Mariottoni, E.B., Datta, S., Dov, D., Jammal, A.A., Berchuck, S.I., Tavares, I.M., Carin, L., Medeiros, F.A.: Artificial Intelligence Mapping of Structure to Function in Glaucoma. Translational Vision Science & Technology **9**(2), 19–19 (03 2020). https://doi.org/10.1167/tvst.9.2.19, https://doi.org/10.1167/tvst.9.2.19
12. Mustafic, N., Ristoldo, F., Nguyen, V., Fraser, C.L., Invernizzi, A., Jamieson, R.V., Grigg, J.R.: Biomarkers in usher syndrome: Ultra-widefield fundus autofluorescence

and optical coherence tomography findings and their correlation with visual acuity and electrophysiology findings. Documenta Ophthalmologica **141**(3), 205–215 (Apr 2020). https://doi.org/10.1007/s10633-020-09765-0
13. Poornachandra, B., Khurana, A.K., Sridharan, P., Chatterjee, P., Jayadev, C., Yadav, N.K., Shetty, R.: Quantifying microstructural changes in retinitis pigmentosa using spectral domain – optical coherence tomography. Eye and Vision **6**(1) (May 2019). https://doi.org/10.1186/s40662-019-0139-0
14. Strang, G., Nguyen, T.Q.: Wavelets and filter banks (1996)
15. Ueda-Consolvo, T., Ozaki, H., Nakamura, T., Oiwake, T., Hayashi, A.: The association between cone density and visual function in the macula of patients with retinitis pigmentosa. Graefe's Archive for Clinical and Experimental Ophthalmology **257**(9), 1841–1846 (Jun 2019). https://doi.org/10.1007/s00417-019-04385-0
16. Wang, Y., Zhang, J., Cavichini, M., Bartsch, D.U.G., Freeman, W.R., Nguyen, T.Q., An, C.: Robust content-adaptive global registration for multimodal retinal images using weakly supervised deep-learning framework. IEEE Transactions on Image Processing **30**, 3167–3178 (2021). https://doi.org/10.1109/TIP.2021.3058570
17. Yassin, S.H., Wang, Y., Freeman, W.R., Heinke, A., Walker, E., Nguyen, T., Bartsch, D.G., An, C., Borooah, S.: Efficacy and accuracy of artificial intelligence to overlay multimodal images from different optical instruments in patients with retinitis pigmentosa. Clinical & Experimental Ophthalmology **51**(5), 446–452 (Apr 2023). https://doi.org/10.1111/ceo.14234